


Assessing Polycystic Kidney Disease in Rodents: Comparison of Robotic 3D Ultrasound and Magnetic Resonance Imaging

Nathan J. Beaumont,¹ Heather L. Holmes,² Adriana V. Gregory,³ Marie E. Edwards,⁴ Juan D. Rojas,¹ Ryan C. Gessner,¹ Paul A. Dayton,⁵ Timothy L. Kline,^{3,4} Michael F. Romero,^{2,3} and Tomasz J. Czernuszewicz^{1,5} 

Abstract

Polycystic kidney disease (PKD) is an inherited disorder characterized by renal cyst formation and enlargement of the kidney. PKD severity can be staged noninvasively by measuring total kidney volume (TKV), a promising biomarker that has recently received regulatory qualification. In preclinical mouse models, where the disease is studied and potential therapeutics are evaluated, the most popular noninvasive method of measuring TKV is magnetic resonance imaging (MRI). Although MRI provides excellent 3D resolution and contrast, these systems are expensive to operate, have long acquisition times, and, consequently, are not heavily used in preclinical PKD research. In this study, a new imaging instrument, based on robotic ultrasound (US), was evaluated as a complementary approach for assessing PKD in rodent models. The objective was to determine the extent to which TKV measurements on the robotic US scanner correlated with both *in vivo* and *ex vivo* reference standards (MRI and Vernier calipers, respectively). A cross-sectional study design was implemented that included both PKD-affected mice and healthy wild types, spanning sex and age for a wide range of kidney volumes. It was found that US-derived TKV measurements and kidney lengths were strongly associated with both *in vivo* MRI and *ex vivo* Vernier caliper measurements ($R^2=0.94$ and 0.90 , respectively). In addition to measuring TKV, renal vascular density was assessed using acoustic angiography (AA), a novel contrast-enhanced US methodology. AA image intensity, indicative of volumetric vascularity, was seen to have a strong negative correlation with TKV ($R^2=0.82$), suggesting impaired renal vascular function in mice with larger kidneys. These studies demonstrate that robotic US can provide a rapid and accurate approach for noninvasively evaluating PKD in rodent models.

KIDNEY360 1: 1128–1136, 2020. doi: <https://doi.org/10.34067/KID.0003912020>

Introduction

Polycystic kidney disease (PKD) is an inherited disease defined by the development of many cysts in the kidneys. The disease is a genetic disorder with autosomal recessive and autosomal dominant forms. The autosomal dominant form is more common and has a prevalence of about one in 2500 people in developed countries (1,2). Cysts tend to increase in number and size over the lifetime of an individual, eventually causing CKD and possible kidney failure (3). To date, only one drug (tolvaptan) is currently approved by the Food and Drug Administration (FDA) to treat PKD and can only slow the progression of the disease (4). Thus, widespread research efforts to create better drugs for PKD are ongoing.

Rodent models play a crucial role in supporting disease research and drug testing environments (5). There are several different small animal models for PKD available today, and disease progression is typically measured terminally with histologic methods

(5,6). Histology provides cellular resolution and can quantify the presence of disease-relevant processes, such as cystic diameter/distribution, inflammation, and fibrosis. However, histology is time consuming and ultimately destructive, limiting it to one time point per subject. In humans, eGFR is a common noninvasive biomarker used to assess renal function. However, in PKD, eGFR tends to decrease at late stages of the disease, where cystic burden is substantial and difficult to treat (7,8). Due to the limitations of eGFR in patients, in 2015 the FDA qualified imaging-derived measures of total kidney volume (TKV) as a biomarker to quantify the efficacy of PKD drugs in clinical trials (9). In addition to earlier sensitivity for disease progression, TKV allows kidneys to be assessed throughout the onset and progression of PKD. In the context of preclinical research, TKV can provide improved statistics between groups with fewer animals required, compared with studies using invasive measurement approaches alone (10).

¹SonoVol, Inc., Durham, North Carolina

²Department of Physiology and Biomedical Engineering, Mayo Clinic, Rochester, Minnesota

³Nephrology and Hypertension, Mayo Clinic, Rochester, Minnesota

⁴Radiology, Mayo Clinic, Rochester, Minnesota

⁵Joint Department of Biomedical Engineering, The University of North Carolina and North Carolina State University, Chapel Hill, North Carolina

Correspondence: Dr. Michael F. Romero, Mayo Clinic College of Medicine, 200 First St SW, Rochester, MN 55905 or Dr. Tomasz J. Czernuszewicz, SonoVol, Inc., 100 Capitola Dr. Suite 240, Durham, NC 27713. Email: Romero.Michael@mayo.edu or tomekc@sonovol.com

The most prevalent methods for noninvasive TKV measurement are magnetic resonance imaging (MRI) and ultrasound (US) because of their excellent soft-tissue contrast, depth of penetration, and lack of ionizing radiation (11). Between the two, MRI has been considered the gold standard because of its high resolution, multiparametric pulse sequencing, and disease-relevant readouts for PKD progression, such as TKV and cystic burden (12–14). However, MRI time points can be expensive due to high operational cost, long acquisition times, and limited access from high user demand. US imaging can provide a cost-effective alternative to MRI for rapid measurement of organ sizes, vascular density, and tissue stiffness, but has long suffered from issues of reproducibility due to its handheld form factor and user dependence. Collecting high-quality, reproducible rodent kidney measurements with US requires experienced sonographers and cumbersome workflows that can negate the cost, time, and throughput efficiencies that are promised by the modality.

Recently, a robotic, preclinical US scanner has been developed to circumvent these challenges. This device uses an automated scanning mechanism to raster a US transducer across the entire body of a rodent, building up a wide-field three-dimensional (3D) image of the anatomy (15). By providing a single 3D image, with a cohesive view of both kidneys within the context of the surrounding anatomy, we hypothesized this technology could provide highly accurate TKV measurements in rodent models of disease. The following study tests this hypothesis in two cross-sectional studies with validation both *in vivo* (i.e., MRI) and *ex vivo* (i.e., Vernier caliper). Additionally, because PKD has been shown to decrease renal vascular density in rodent models (16,17), we evaluated whether this reduction in density could be assessed with a microbubble contrast-enhanced microvascular imaging mode provided by the robotic instrument (acoustic angiography [AA]) (18). Finally, intra- and inter-rater reliability was assessed and reported.

Materials and Methods

Imaging Studies

Two different cohorts of mice were used in this study, one to compare the robotic US instrument, with reference

standard *in vivo* imaging systems, and one to compare the robotic US system with an *ex vivo* standard (Vernier calipers). Robotic US scans (Figure 1) were captured with a Vega imager (SonoVol, Inc., Durham, NC), and compared with both MRI (16.4T Avance DRX 700WB; Bruker BioSpin, Billerica, MA) and conventional preclinical US (Vevo 3100; FUJIFILM VisualSonics Inc., Toronto, Canada). All studies were approved by the institutional animal care and use committees of University of North Carolina at Chapel Hill (UNC) and Mayo Clinic. More details about scanning parameters can be found in the Supplemental Material, and an example of robotic US scanning is provided in Supplemental Video 1.

Cohort 1

To evaluate the accuracy of the robotic US scanner against the reference standard *in vivo* imaging, a cross-sectional study design was used, ensuring that kidneys over a range of sizes would be observed. Male and female PKD mice ($N=7$) were first imaged at the Mayo Clinic with both MRI and conventional US, per standard protocols, to serve as the gold standard. These animals were then transported to UNC for imaging with the robotic US instrument. Specific details on the imaging parameters for MRI and US can be found in the Supplemental Methods. Additionally, physical and genetic characteristics of cohort 1 are provided in Supplemental Table 1.

Cohort 2

To evaluate *in vivo* versus *ex vivo* size measurements, a second cohort ($N=8$) of healthy Nu/Nu mice were used (Charles River Laboratories, Wilmington, MA). The cohort contained both female and male mice at two different ages (4 weeks old and 16 weeks old). These animals were imaged exclusively with the robotic US scanner at UNC and were not transported to any other facility. After robotic US acquisition of cohort 2, all mice were euthanized to assess kidney size with Vernier calipers (Mitutoyo, Sakado, Japan) postnecropsy. Additionally, the extracted kidneys were imaged on the robotic US scanner after Vernier measurements to confirm accuracy of *in vivo* measurements in the absence of surrounding anatomy. Excised kidneys were placed in

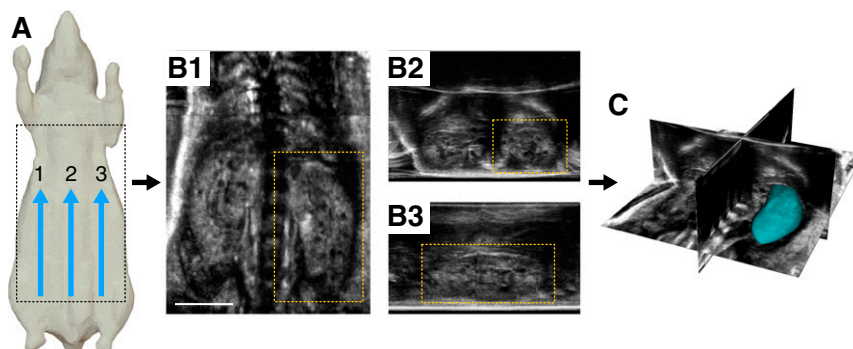


Figure 1. | An overview of the acquisition workflow for the robotic ultrasound system. (A) Multiple parallel sweeps are acquired, usually three, resulting in thousands of individual two-dimensional images from across the animal's body. (B and C) These images are then stitched together to produce a single wide-field three-dimensional (3D) image volume, which can be viewed in different orientations. The 3D data can be seen in (B1) frontal, (B2) transverse, and (B3) sagittal planes, respectively. (C) Each kidney can then be segmented in 3D to assess total kidney volume. Scale bar, 1 cm.

warmed US gel on the Vega imager and scanned in 3D, using the same imaging parameters as was done *in vivo*.

Image Analysis

To determine kidney volume from a 3D image, kidneys were manually segmented from the data. Rapid segmentation from the robotic US data was performed using SonoEQ (SonoVol, Inc.), which uses an open-source back end of 3D Slicer (www.slicer.org) (19). To enhance kidney border delineation in the US data, the 3D volumes from both US transducers (dual element and linear array) were overlaid on one other with alpha blending. MRI and conventional US volumes were segmented by two separate readers, using segmentation software developed in house (20). For the duration of image analysis, all readers were blinded to animal genotypes, sex, age, and one another's kidney volume *via* mouse label randomization. For intermodality assessment (US versus MRI) and intramodality assessment (robotic US versus conventional US), the segmentations from one expert reader were compared across all three categories: robotic US (R.C.G.), conventional US (H.L.H.), and MRI (M.E.E.). To determine accuracy of kidney sizing of the robotic US system compared with *ex vivo* measurements, all kidneys in cohort 2 were assessed in two ways: with software calipers and 3D segmentations. Software calipers are linear measurement objects, which can be placed within 3D images using SonoEQ software, and were used to measure the length and width of the kidneys in the same orientation as the Vernier calipers postnecropsy. To assess inter-reader reliability for the robotic US scanner, four independent readers (N.J.B., J.D.R., R.C.G., and T.J.C.), spanning a range of US imaging expertise, segmented kidneys in the robotic US data and were compared. To assess intrareader variability, one reader (N.J.B.) segmented the same kidney volumes again 67 days later, without viewing previous segmentations. To quantify minimum detectable cyst size, a single coronal slice of kidneys with many cysts had digital caliper measurements made for 11 identifiable cysts.

Assessing Relationship between Kidney Vascularity and Kidney Size

To assess the relationship between kidney size and kidney vascularity, an image intensity analysis was performed on AA images of each kidney. The US segmentations for each kidney, described in the previous section, were applied to the coregistered AA volumes. This allowed the image voxels within the kidney to be analyzed as a histogram of intensity values. Because the brightness of a given pixel is correlated with the amount of microbubble contrast agents present in that localized region of tissue, the "percent positivity," or percentage of pixels within a region of interest above a given threshold, is a proxy for vascularity. This metric of vascularity necessitated the selection of an intensity threshold above which pixels were identified to represent vasculature. By modulating the "vascularity threshold" across a range, the strength of the correlation between kidney size and vascularity could be assessed. This analysis was performed in Matlab R2017a (Mathworks, Natick, MA).

Statistical Analyses

Agreement and correlation between imaging modalities was assessed in Matlab R2017a (Mathworks) using Klein's Bland–Altman and Correlation Plot toolbox version 1.10. Reported metrics included Pearson correlation coefficient (r), Pearson squared (r^2), coefficient of determination (R^2), Spearman correlation coefficient (ρ), line of best fit equation (least squares), coefficient of variation, and limits of agreement (LOA). The linear regression equation was solved with a zero-intercept boundary condition. Bias between measurements was assessed using a Bland–Altman analysis. $P < 0.05$ was considered statistically significant. To quantify inter-reader reliability, the intraclass correlation coefficient (ICC), using the absolute agreement among measurements ("ICC [A,1]") formulation (21), was computed across the four image readers, and so was the coefficient of variation between US measurements for each TKV.

Results

Evaluating Kidney Size Measurement Accuracy (*In Vivo* Studies)

Kidneys could be readily visualized in both MRI and robotic US datasets. As expected, the MRI datasets had better tissue contrast, but required more acquisition time per animal (5–10 minutes versus 26 seconds). When compared side by side, the MRI and robotic US images had corresponding anatomic landmarks within each volume, such as cysts and blood vessels (Figure 2). Many cysts, down to 0.4 mm in diameter, were identifiable in US, but smaller cysts were not confidently distinguishable from US speckle (Supplemental Figure 1).

To assess the correlation between MRI and the robotic US scanner, segmented kidneys from cohort 1 were compared *via* a linear regression and Bland–Altman analysis (Figure 3). The correlation between the segmentations between modalities was very strong, with an R^2 value of 0.94. Bland–Altman analysis revealed a mean underestimation bias of kidney volume by 4.9 mm^3 with robotic US; however, it was not found to be significant ($P = 0.62$). The LOA between the two modalities was 70 mm^3 . Additionally, robotic US was compared with conventional US (Supplemental Figure 2), and conventional US with MRI (Supplemental Figure 3). When compared against conventional US, robotic US demonstrated excellent correlation ($R^2 = 0.97$) and an even smaller LOA (44 mm^3) as compared with MRI. Conventional US and MRI showed a high degree of correlation as well ($R^2 = 0.92$), albeit with a larger LOA (90 mm^3).

Evaluating Kidney Size Measurement Accuracy (*Ex Vivo* Studies)

To evaluate the relationship between *in vivo* kidney size measurements made on the robotic US scanner and *ex vivo* methods for sizing kidneys *via* Vernier calipers, a comparison study was performed on cohort 2, including measurements for kidney width and length. For the robotic US scanner dataset, 3D images were acquired on both *in vivo* kidneys before necropsy (serving as the normal scenario for measurement in a longitudinal study), and explanted kidneys postnecropsy (serving as the best case scenario for system performance and measurement accuracy). Figure 4 illustrates the placement of calipers (Vernier calipers in

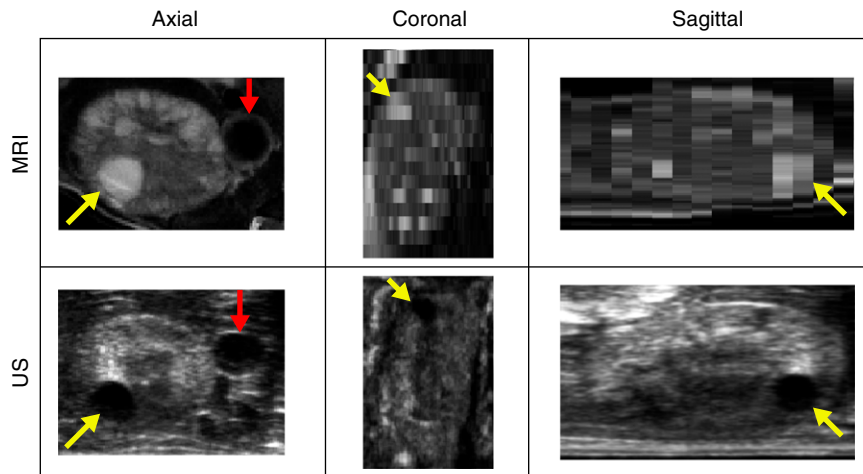


Figure 2. | A side by side comparison of an US scan versus an MRI scan of a kidney. Slices at the same location in both imaging modalities show cysts (yellow arrows) in the same regions. The inferior vena cava is also visible (red arrow).

Figure 4A, and US calipers in Figure 4, B and C, for *in vivo* and *ex vivo*, respectively). As measured by Vernier calipers, the range in kidney widths for this study was 5.42–8.03 mm, and the range in kidney lengths was 7.47–11.75 mm. Kidney dimensions measured with ultrasonic calipers, both *in vivo* and *ex vivo*, were strongly correlated with Vernier caliper measurements, with coefficients of determination of $R^2=0.90$ and $R^2=0.95$, respectively (Figure 4). The expected trends for age and sex were also observed: older mice had larger kidneys than younger mice for the same sex, and males, on average, had larger kidneys than the females for a given age (Supplemental Figure 4).

Evaluating Consistency between Readers

Figure 5 illustrates inter-reader variability in TKV for the cohort 1 mice scanned on the robotic US system, sorted by size. The mean and SD of the measurements are indicated,

and so is the values of each of the four readers. The range in TKV for this cohort was 250.5–904.8 mm³. On average, the SD for a TKV measurement across multiple readers was 43.62 mm³, with a minimum of 19.5 mm³ and maximum of 69.0 mm³ for animals 603 and 60A, respectively. The mean coefficient of variation (SD/mean) for these mice was 9%, with a minimum of 3% and maximum of 18% for mice 570B and 607, respectively. The ICC between the four readers was very strong at 0.93 (95% CI, 0.83 to 0.97). As for intrauser variability, the tested reader had an ICC of 0.96 (95% CI, 0.88 to 0.99) between the two time points.

Evaluating the Relationship between Kidney Vasculature and Kidney Size

It was hypothesized that, in AA images, there would be a correlation between the percentage of bright pixels within

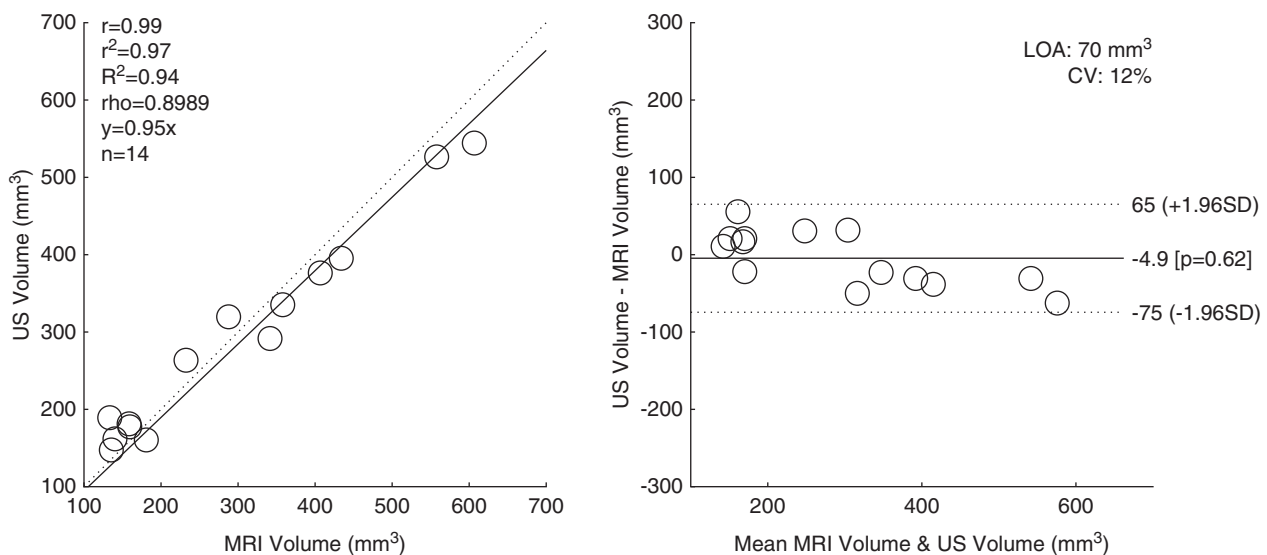


Figure 3. | Regression and Bland–Altman plots comparing robotic ultrasound–based *in vivo* measurements of kidney volume with *in vivo* MRI. CV, coefficient of variation; LOA, limits of agreement; *r*, Pearson correlation coefficient; *r*², Pearson coefficient squared; *R*², coefficient of determination; *rho*, Spearman correlation coefficient.

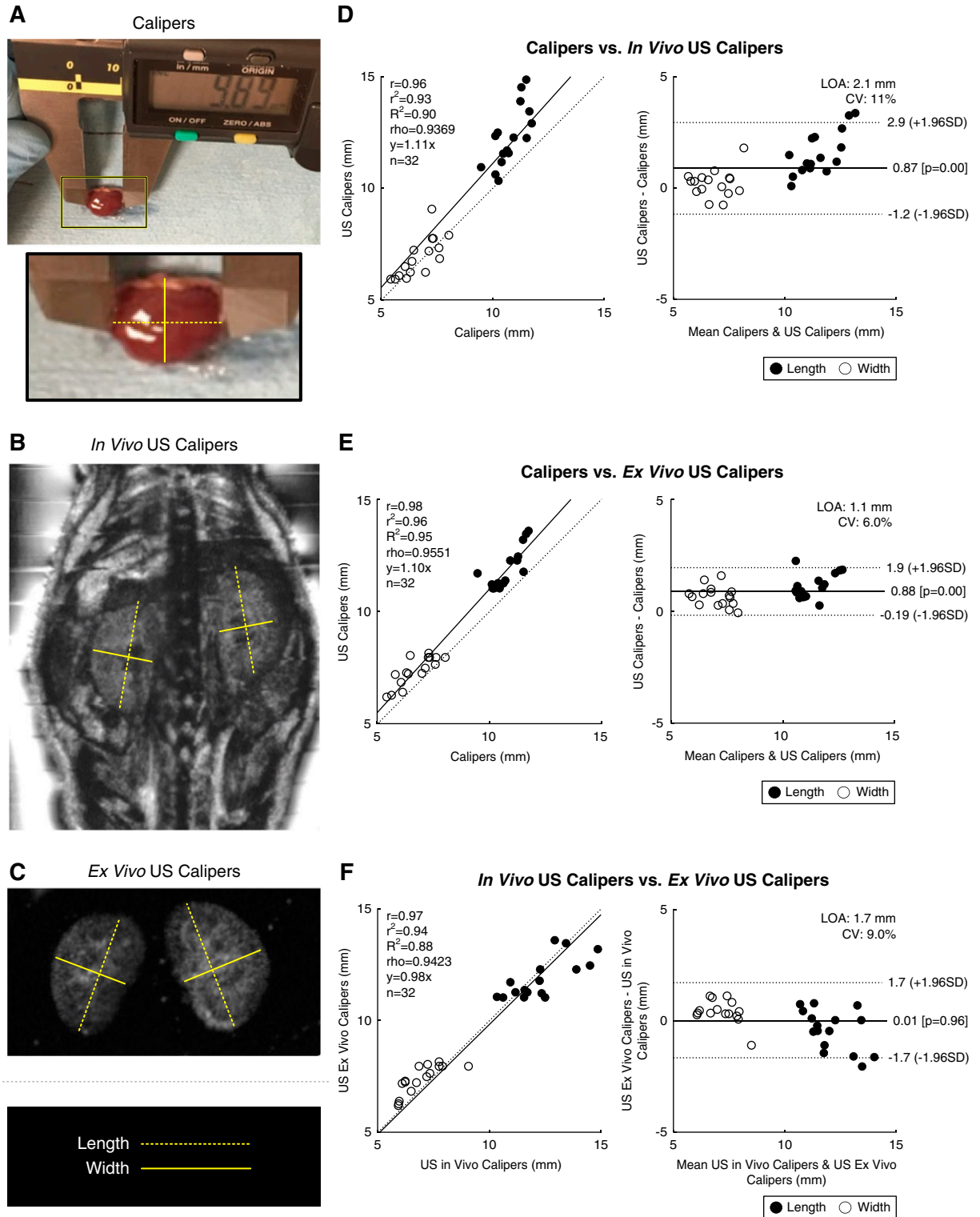


Figure 4. | Vernier calipers versus US calipers. (A) An image showing how Vernier calipers were used to measure kidney length (dashed line) and width (solid line). (B) US calipers drawn in software over a coronal *in vivo* US image. (C) US calipers drawn over a US image of *ex vivo* kidneys. Lines in (A, B, and C) correspond to the same axes. (D–F) Bland–Altman plots comparing (D) *in vivo* US calipers, (E) *ex vivo* US calipers, and (F) *ex vivo* Vernier calipers. CV, coefficient of variation; LOA, limits of agreement; r , Pearson correlation coefficient; r^2 , Pearson coefficient squared; R^2 , coefficient of determination; ρ , Spearman correlation coefficient.

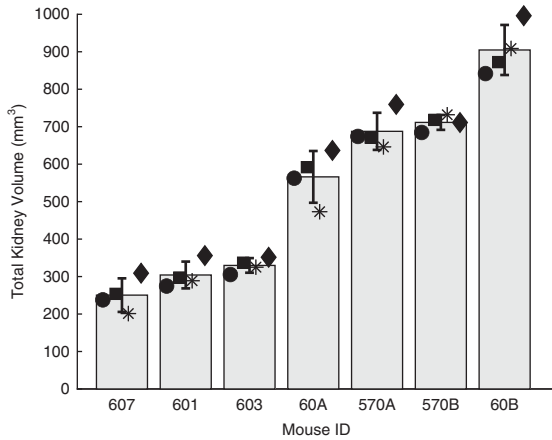


Figure 5. | Inter-reader variability for total kidney volume measurements for cohort 1. Readers are indicated by the marker, with mean and SDs plotted. ID, identifier.

the kidney (percent positivity, *i.e.*, vascularity) and the kidney’s size. For instance, a kidney filled with large, non-vascularized cysts would contain a high percentage of low-intensity pixels within the kidney’s interior, and thus a low

percent positivity. Conversely, a kidney with high vascular density would have a high percent positivity. The optimal threshold yielding the maximum strength of correlation between vascularity and kidney size was an AA intensity value of 46 (a post-thresholded image at this value can be seen in Figure 6A). At this threshold value, the R^2 value for the linear regression between vascularity and kidney size was 0.82. This analysis was exploratory in nature, and additional studies need to be performed to characterize the stability of this optimal threshold across different cohorts of animals, and how this can be used to extract other meaningful read-outs from PKD models, such as cystic burden.

Discussion

In this study, it was demonstrated that robotic 3D US can produce accurate and consistent *in vivo* measurements of TKV in rodent models. Correlation analyses between robotic US- and MRI-derived kidney volume yielded an R^2 value of 0.94, with no statistically significant bias. Furthermore, robotic US measurements were in very good agreement with conventional US measurements ($R^2=0.97$) and required substantially less time to acquire. This is a significant finding, because it illustrates that the new US instrument with a robotic form factor can be used as

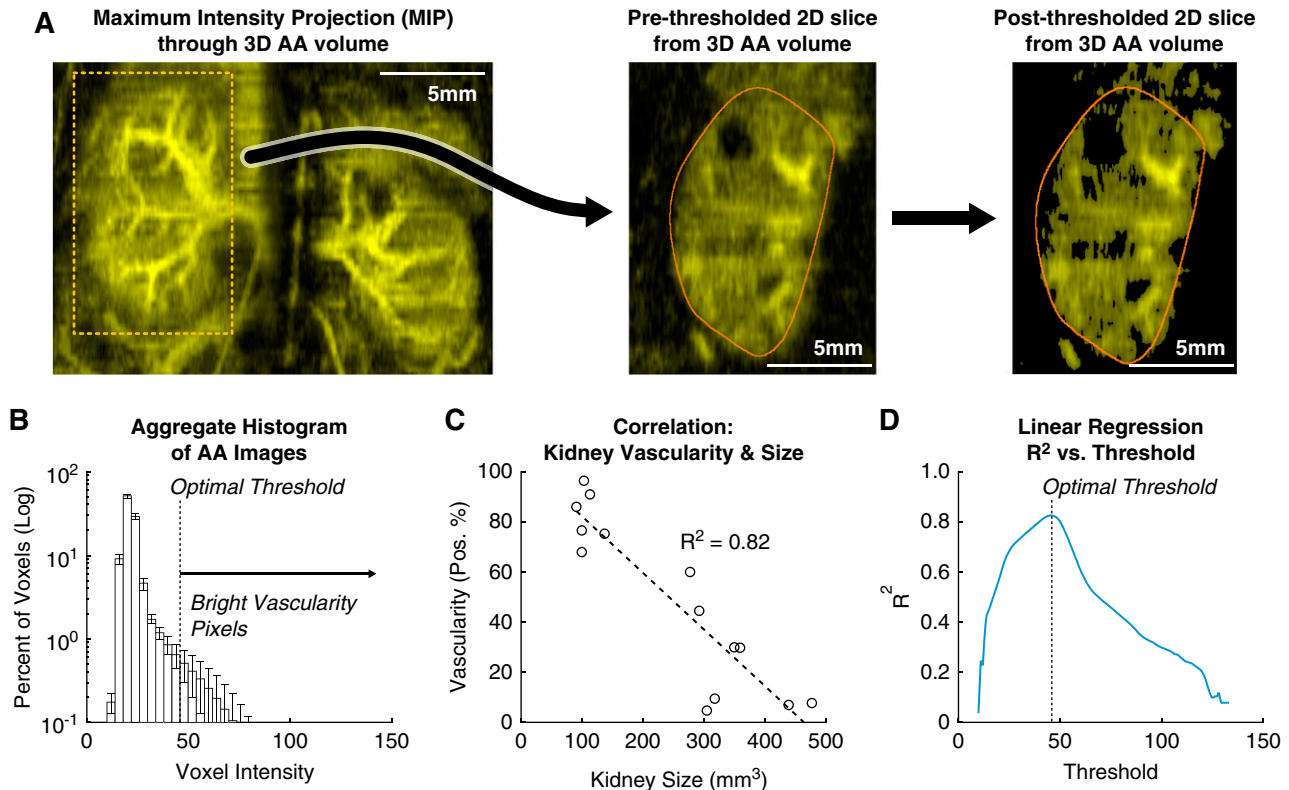


Figure 6. | Correlation between kidney vascularity and kidney size. (A) Vessel morphology as visualized *via* maximum intensity projections of acoustic angiography (AA) volumes. A single two-dimensional (2D) slice of the volume with an exemplary cyst (white arrow) is shown. After thresholding at the optimal threshold of 46 counts, the voxels within the cyst, and elsewhere, have been set to zero and are not included in the percent positivity metric for vascularity. (B) Mean histogram of all AA volumes of cohort 1. SDs of the histogram bins are shown with error bars. (C) The percent of bright voxels in a kidney during microbubble perfusion (positivity %) negatively correlates with kidney volume. In this plot, the kidneys were thresholded at 46 counts. (D) The coefficient of determination of the linear regression in (C) depends on the thresholding level. Thresholding at 46 counts gives the highest R^2 value. This threshold excludes cysts but includes most vasculature (seen on the right in [A]).

a high-throughput screening method for TKV, thus enabling large-cohort preclinical studies that would otherwise be cost/time prohibitive to perform with MRI or conventional US. When higher spatial resolution is desired, individual animals screened by US can always be selectively sent for MRI, similar to targeted recruitment in clinical studies. In addition to high correlation of kidney volume measurements between the modalities, cysts down to 0.4 mm in diameter were visible in both (Figure 2, Supplemental Figure 1). This suggests that longitudinal monitoring of total cyst volume, mean cyst size, and percent cyst space could be possible with robotic US. Other metrics to quantify PKD, such as parenchymal fibrosis and renal blood flow, could also be measured with robotic US *via* shear wave elastography imaging and Doppler imaging, respectively. Although these metrics were beyond the scope of our single-time-point validation study, they will be explored in more detail in the future.

Additionally, it was demonstrated that wild-type kidney sizes measured *in vivo* with the robotic US system were highly correlated with kidney sizes measured *ex vivo* (Figure 4). *Ex vivo* organ sizing is a routine practice in preclinical research because noninvasive imaging is typically not conducted. Specifically, for the kidney, this can be done *via* volume-displacement approaches or caliper measurements performed in either two axes (*i.e.*, length and width) or three axes (*i.e.*, length, width, and height) that can be fit to an ellipsoidal equation to yield volume (22). In this study, *in vivo* measurements were compared against *ex vivo* measurements made by both ultrasonic and manual means (*via* Vernier calipers). In all cases, caliper measurements matched closely, with R^2 values ranging from 0.88 to 0.95.

Interestingly, a positive bias was observed when comparing *in vivo* US calipers with Vernier calipers (0.87 mm, $P=5.0e-5$; Figure 4D). To determine if this was an artifact of the US reader seeing the border of the kidney incorrectly within the *in vivo* US data, we analyzed the measurements between Vernier calipers and *ex vivo* US calipers where the tissue borders have maximum contrast against the coupling gel. In this case (Figure 4E), nearly the same overestimation of 0.88 mm by US can be seen ($P=2.9e-10$). One explanation for this could be that the Vernier calipers were physically compressing the kidneys by this distance, causing an underestimation in these data, which is a known challenge with using Vernier calipers for measuring tissue samples. When comparing the *in vivo* versus *ex vivo* US calipers, measurements were highly consistent with no significant bias (Figure 4F).

This study found that kidney vascularity, as measured by bright contrast-enhanced voxels, had a strong negative correlation to kidney volume as measured by US scans ($R^2=0.82$) (Figure 6). Although microbubbles are generally considered safe for use both clinically and preclinically (23), using them in concert with high-intensity US pulses can result in unwanted bioeffects and cellular damage. In rodent kidneys, the mechanical index (MI) threshold at which microbubble damage occurs has been found to depend on frame rate and imaging time of an area. One study found that imaging one location for 60 seconds at one frame per second with an MI >0.6 can cause glomerular hemorrhage (24). Another larger study found no glomerular hemorrhage at an MI up to 1.9, but did find BUN increased with pulses at

1.0 MI (25). Because the Vega system performs AA at an MI of 0.54, and rapidly translates the transducer across the kidney, it is not expected that significant bioeffects, as reported in previous studies, would occur from a kidney vasculature scan; however, this hypothesis should be rigorously tested in future studies.

PKD in humans usually causes hypertension (26, 27, 28), and cardiovascular disease is the most common cause of death for patients with PKD (29). In addition to hypertension, cardiovascular abnormalities, such as left ventricular hypertrophy, biventricular diastolic dysfunction, and impaired coronary flow velocity reserve, can develop (30). US is routinely used to rapidly measure common cardiovascular metrics like ejection fraction, stroke volume, and cardiac output. In future studies, it would be possible to measure TKV along with these cardiac metrics using the robotic US scanner evaluated herein.

One issue that is often problematic with *in vivo* imaging is respiratory artifacts. In this study, animal respiration was not found to cause significant artifacts in US kidney scans. In Figure 1 (panel B1), horizontal lines are evident on the skin of the mouse where breaths occurred, but are miniscule on the kidneys. This is because, firstly, animals lay supine so the kidney displacement from lung expansion was negligible. Secondly, a high- and low-frequency scan was overlaid for segmentation, so the respiratory lines became less sharp. Based on these results, it does not appear that active respiration gating is necessary for accurate TKV measurement, which allows for a less complicated workflow and higher animal throughput.

There were several limitations to this study. First, the MRI and US imaging was not performed at the same facility, requiring mice to be shipped and acclimated, which incurred a time delay between imaging modalities. Although this delay was relatively short (20 days), it is conceivable that the kidney size may have changed, due to natural biologic progression, and reduced the agreement between MRI and US. Second, the MRI and US datasets were evaluated by different readers using different segmentation software packages, with no explicit training between the two. It is expected that, with improved training (*e.g.*, developing a segmentation rubric), the correlation between MRI and US could increase beyond that reported in this study. Third, *ex vivo* kidney volume measurements were observed to have a time dependence with time of euthanasia (Supplemental Figure 5). In this study, all mice in cohort 2 were euthanized *via* isoflurane overdose followed by cervical dislocation, with kidney extraction times varying depending on the speed of the technician performing the necropsies. The first kidneys extracted had *ex vivo* volumes that measured smaller than *in vivo* volumes, whereas the last kidneys extracted (approximately 30 minutes post-euthanasia) had *ex vivo* volumes larger than the *in vivo* volume. This indicates that post-mortem changes may have had an effect on the correlation between *in vivo* and *ex vivo* measurements and highlights the importance of necropsy standardization. Fourth, this study only evaluated a small number of mice ($N=30$ kidneys between the two cohorts), so larger studies with a broader range of kidney sizes and disease pathologies (*e.g.*, kidney fibrosis models) should be conducted in the future. Finally, serum and urinary biomarkers with PKD progression prediction similar to TKV, such as $\beta 2$

microglobulin and monocyte chemoattractant protein-1 (31), were not measured in this study but would provide more detailed disease stratification in future studies.

Disclosures

N. Beaumont, T. Czernuszewicz, P. Dayton, R. Gessner, and J. Rojas are either employed by, have a significant financial interest in, or are coinventors on patents licensed by SonoVol, Inc. Authors report the following National Institutes of Health (NIH) grant with SonoVol is under consideration: R43 DK126607 (Small Business Innovation Research/NIH; multiple principal investigator [MPI]; SonoVol principal investigator, T. Czernuszewicz/Mayo; Mayo MPI, T. Kline and M. Romero), “A new robotic AI imaging platform for improved kidney disease research and drug discovery.” This proposal builds on and extends the work presented in this manuscript.

Funding

Funding for this work was provided by the Mayo Foundation, the Oxalosis & Hyperoxaluria Foundation, and the Mayo Translational PKD Center grant P30 DK090728.

Acknowledgments

We would like to acknowledge Mr. Brian Velasco, and the University of North Carolina Animal Core for their assistance with animal handling during the *in vivo* experiments.

Author Contributions

N. Beaumont wrote the original draft and was responsible for visualization; N. Beaumont, T. Czernuszewicz, P. Dayton, R. Gessner, H. Holmes, T. Kline, J. Rojas, and M. Romero reviewed and edited the manuscript; N. Beaumont, T. Czernuszewicz, M. Edwards, R. Gessner, A. Gregory, H. Holmes, and J. Rojas were responsible for formal analysis; T. Czernuszewicz was responsible for methodology; T. Czernuszewicz, P. Dayton, R. Gessner, T. Kline, and M. Romero were responsible for resources and supervision; T. Czernuszewicz, M. Edwards, A. Gregory, and H. Holmes were responsible for data curation; A. Gregory was responsible for software; T. Czernuszewicz, R. Gessner, T. Kline, and M. Romero conceptualized the study; T. Czernuszewicz, R. Gessner, and M. Romero were responsible for funding acquisition; and M. Romero was responsible for project administration.

Supplemental Material

This article contains supplemental material online at <http://kidney360.asnjournals.org/lookup/suppl/doi:10.34067/KID.K3602020000391/DCSupplemental>.

Supplemental Figure 1. Analysis of cystic diameter measured from a representative coronal plane.

Supplemental Figure 2. Regression and Bland-Altman plots comparing *in vivo* measurements of kidney volume between robotic ultrasound to conventional ultrasound (“Vega” and “Vevo” systems, respectively).

Supplemental Figure 3. Regression and Bland-Altman plots comparing *in vivo* measurements of kidney volume between conventional ultrasound to MRI.

Supplemental Figure 4. Comparing *in vivo* to *ex vivo* kidney volumes measured with robotic US scans.

Supplemental Figure 5. Scatter plot showing the difference between *in vivo* and *ex vivo* kidney volume as function of time post euthanasia.

Supplemental Table 1. Mice Used for In Vivo MRI Validation Studies (Cohort 1)

Supplemental Video 1. ROI placement and data acquisition workflow of the Vega robotic US scanner.

References

- Levy M, Feingold J: Estimating prevalence in single-gene kidney diseases progressing to renal failure. *Kidney Int* 58: 925–943, 2000
- Willey CJ, Blais JD, Hall AK, Krasa HB, Makin AJ, Czerwiec FS: Prevalence of autosomal dominant polycystic kidney disease in the European Union. *Nephrol Dial Transplant* 32: 1356–1363, 2017
- Igarashi P, Somlo S: Polycystic kidney disease. *J Am Soc Nephrol* 18: 1371–1373, 2007
- Sans-Atxer L, Joly D: Tolvaptan in the treatment of autosomal dominant polycystic kidney disease: Patient selection and special considerations. *Int J Nephrol Renovasc Dis* 11: 41–51, 2018
- Nagao S, Kugita M, Yoshihara D, Yamaguchi T: Animal models for human polycystic kidney disease. *Exp Anim* 61: 477–488, 2012
- Happé H, Peters DJM: Translational research in ADPKD: Lessons from animal models. *Nat Rev Nephrol* 10: 587–601, 2014
- Perrone RD, Mouksassi M-S, Romero K, Czerwiec FS, Chapman AB, Gitomer BY, Torres VE, Miskulin DC, Broadbent S, Marier JF: Total kidney volume is a prognostic biomarker of renal function decline and progression to end-stage renal disease in patients with autosomal dominant polycystic kidney disease [published correction appears in *Kidney Int Rep* 3: 1015, 2018 10.1016/j.ekir.2018.05.006]. *Kidney Int Rep* 2: 442–450, 2017
- Grantham JJ, Torres VE: The importance of total kidney volume in evaluating progression of polycystic kidney disease. *Nat Rev Nephrol* 12: 667–677, 2016
- US Food and Drug Administration, Center for Drug Evaluation and Research: Qualification of biomarker total kidney volume in studies for treatment of autosomal dominant polycystic kidney disease guidance for industry, 2016. Available at: <https://www.fda.gov/regulatory-information/search-fda-guidance-documents/qualification-biomarker-total-kidney-volume-studies-treatment-autosomal-dominant-polycystic-kidney>. Accessed August 24, 2020
- Bidar AW, Ploj K, Lelliott C, Nelander K, Winzell MS, Böttcher G, Oscarsson J, Storlien L, Hockings PD: In vivo imaging of lipid storage and regression in diet-induced obesity during nutrition manipulation. *Am J Physiol Metab* 303: E1287–E1295, 2012
- Tangri N, Hougen I, Alam A, Perrone R, McFarlane P, Pei Y: Total kidney volume as a biomarker of disease progression in autosomal dominant polycystic kidney disease. *Can J Kidney Heal Dis* 4: 2054358117693355, 2017
- Edwards ME, Blais JD, Czerwiec FS, Erickson BJ, Torres VE, Kline TL: Standardizing total kidney volume measurements for clinical trials of autosomal dominant polycystic kidney disease. *Clin Kidney J* 12: 71–77, 2019
- Kline TL, Edwards ME, Garg I, Irazabal MV, Korfiatis P, Harris PC, King BF, Torres VE, Venkatesh SK, Erickson BJ: Quantitative MRI of kidneys in renal disease. *Abdom Radiol (NY)* 43: 629–638, 2018
- Wallace DP, Hou Y-P, Huang ZL, Nivens E, Savinkova L, Yamaguchi T, Bilgen M: Tracking kidney volume in mice with polycystic kidney disease by magnetic resonance imaging. *Kidney Int* 73: 778–781, 2008
- Czernuszewicz TJ, Papadopoulou V, Rojas JD, Rajamahendiran RM, Perdomo J, Butler J, Harlacher M, O’Connell G, Zukić D, Aylward SR, Dayton PA, Gessner RC: A new preclinical ultrasound platform for widefield 3D imaging of rodents. *Rev Sci Instrum* 89: 075107, 2018
- Xu R, Franchi F, Miller B, Crane JA, Peterson KM, Psaltis PJ, Harris PC, Lerman LO, Rodriguez-Porcel M: Polycystic kidneys have decreased vascular density: A micro-CT study. *Microcirculation* 20: 183–189, 2013
- Ogunlade O, Connell JJ, Huang JL, Zhang E, Lythgoe MF, Long DA, Beard P: *In vivo* three-dimensional photoacoustic imaging of the renal vasculature in preclinical rodent models. *Am J Physiol Renal Physiol* 314: F1145–F1153, 2018

18. Gessner RC, Frederick CB, Foster FS, Dayton PA: Acoustic angiography: A new imaging modality for assessing microvasculature architecture. *Int J Biomed Imaging* 2013: 936593, 2013
19. Fedorov A, Beichel R, Kalpathy-Cramer J, Finet J, Fillion-Robin J-C, Pujol S, Bauer C, Jennings D, Fennessy F, Sonka M, Buatti J, Aylward S, Miller JV, Pieper S, Kikinis R: 3D slicer as an image computing platform for the quantitative imaging network. *Magn Reson Imaging* 30: 1323–1341, 2012
20. Kline TL, Edwards ME, Korfiatis P, Akkus Z, Torres VE, Erickson BJ: Semiautomated segmentation of polycystic kidneys in T2-weighted MR images. *AJR Am J Roentgenol* 207: 605–613, 2016
21. McGraw KO, Wong SP: Forming inferences about some intraclass correlation coefficients. *Psychol Methods* 1: 30–46, 1996
22. Chao K, Liao K, Khan M, Shi C, Li J, Goldberg ID, Narayan P: An improved method for estimating renal dimensions; implications for management of kidney disease. *Appl Sci (Basel)* 9: 3198, 2019
23. Chong Wui K., Papadopoulou Virginie, Dayton Paul A.: Imaging with ultrasound contrast agents: current status and future. *Abdom Radiol* 43[4]: 762–772, 2018
24. Miller Douglas L., Dou Chunyan, Wiggins Roger C., Wharram Bryan L., Goyal Meera, Williams Alun R.: An in vivo rat model simulating imaging of human kidney by diagnostic ultrasound with gas-body contrast agent. *Ultrasound in Medicine & Biology* 33[1]: 129–135, 2007
25. Nyankima A. Gloria, Kasoji Sandeep, Cianciolo Rachel, Dayton Paul A., Chang Emily H.: Histological and blood chemistry examination of the rodent kidney after exposure to flash-replenishment ultrasound contrast imaging. *Ultrasonics* 98: 1–6, 2019
26. Chapman AB, Stepniakowski K, Rahbari-Oskoui F: Hypertension in autosomal dominant polycystic kidney disease. *Adv Chronic Kidney Dis* 17: 153–163, 2010
27. Bergmann C: ARPKD and early manifestations of ADPKD: The original polycystic kidney disease and phenocopies. *Pediatr Nephrol* 30: 15–30, 2015
28. Chapman AB, Guay-Woodford LM, Grantham JJ, Torres VE, Bae KT, Baumgarten DA, Kenney PJ, King BF Jr., Glockner JF, Wetzel LH, Brummer ME, O'Neill WC, Robbin ML, Bennett WM, Klahr S, Hirschman GH, Kimmel PL, Thompson PA, Miller JP; Consortium for Radiologic Imaging Studies of Polycystic Kidney Disease cohort: Renal structure in early autosomal-dominant polycystic kidney disease (ADPKD): The consortium for radiologic imaging studies of polycystic kidney disease (CRISP) cohort. *Kidney Int* 64: 1035–1045, 2003
29. Rahman E, Niaz FA, Al-Suwaidia A, Nahrir S, Bashir M, Rahman H, Hammad D: Analysis of causes of mortality in patients with autosomal dominant polycystic kidney disease: A single center study. *Saudi J Kidney Dis Transpl* 20: 806–810, 2009
30. Ecker T, Schrier RW: Cardiovascular abnormalities in autosomal-dominant polycystic kidney disease. *Nat Rev Nephrol* 5: 221–228, 2009
31. Messchendorp AL, Meijer E, Visser FW, Engels GE, Kappert P, Losekoot M, Peters DJM, Gansevoort RT; on behalf of the DIPAK-1 study investigators: Rapid progression of autosomal dominant polycystic kidney disease: Urinary biomarkers as predictors. *Am J Nephrol* 50: 375–385, 2019

Received: June 24, 2020 **Accepted:** August 17, 2020